# Identification of Gas-phase Pyrolysis Products in a Prescribed Fire: First Detections Using Infrared Spectroscopy for Naphthalene, Methyl Nitrite, Allene, Acrolein and Acetaldehyde**

Nicole K. Scharko[1], Ashley M. Oeck[1], Russell G. Tonkyn[1], Stephen P. Baker[2],
Emily N. Lincoln[2], Joey Chong[3], Bonni M. Corcoran[3], Gloria M. Burke[3], David R. Weise[3],
Tanya L. Myers[1], Catherine A. Banach[1], and Timothy J. Johnson[1*]

[1]Pacific Northwest National Laboratories, Richland, WA, USA
[2]USDA Forest Service, Rocky Mountain Research Station, Missoula, MT, USA
[3]USDA Forest Service, Pacific Southwest Research Station, Riverside, CA, USA

*To whom correspondence should be addressed: Timothy.Johnson@pnnl.gov

## ABSTRACT

Volatile organic compounds (VOCs) are emitted from many sources, including wildland fire. VOCs have received heightened emphasis due to such gases' influential role in the atmosphere, as well as possible health effects. We have used extractive infrared (IR) spectroscopy on recent prescribed burns in longleaf pine stands and herein report the first detection of five compounds using this technique. The newly reported IR detections include naphthalene, methyl nitrite, allene, acrolein and acetaldehyde. We discuss the approaches used for detection, particularly the software methods needed to fit the analyte and multiple (interfering) spectral components within the selected spectral micro-window(s). We also discuss the method's detection limits and related parameters such as spectral resolution.

## 1. INTRODUCTION

Wildland fire releases significant quantities of trace gases into the environment (Akagi et al., 2011; Andreae et al., 2001; Crutzen et al., 1979; Yokelson et al., 2013; Andreae, 1991), and such gases can profoundly influence atmospheric chemistry (Crutzen et al., 1990). In some parts of the world, wildfires are becoming more prevalent as well as increasing in impact (Turetsky et al., 2011; Miller et al., 2009). Additionally, prescribed burning is used as a preventive tool to reduce hazardous fuel buildups in an effort to reduce or eliminate the risk of such wildfires (Fernandes et al., 2003). Understanding the products associated with the burning of biomass has received considerable attention since the emissions can markedly impact the atmosphere. Fourier transform infrared (FTIR) spectroscopy is one technique that has been extensively used to identify and quantify gases emitted from burns, generally used in either an open path configuration (Burling et al., 2010; Akagi et al., 2014; Selimovic et al., 2018; Stockwell et al., 2014) or as an extractive method (Burling et al., 2011; Akagi et al., 2013; Akagi et al., 2014). Extractive systems typically use a long-path gas cell coupled to an FTIR instrument so as to increase the sensitivity. Such approaches have been quite successful; an increasing number of species continue to be identified and quantified due to the availability of reference gas-phase spectral libraries such as the PNNL spectral library (Sharpe et al., 2004) or the HITRAN database (Gordon et al., 2017). Such libraries contain absorption cross-sections that make it possible to obtain quantitative results (i.e. mixing ratios) without the need for calibration gases. To the best of our knowledge, the actual list of biomass burning chemical species measured by FTIR has remained limited to ca. 36 compounds (Table 1); one goal of our research was to expand the list of chemical species to which infrared methods could be applied. All of the compounds detailed in this study have in fact been previously detected using other analytical methods (Akagi et al., 2013; Gilman et al., 2015; Karl et al., 2007; Koss et al.,

2

49  2018; Yokelson et al., 2009) such as proton-transfer-reaction time-of-flight mass spectrometry

50  (PTR-ToF) (Koss et al., 2018) or gas chromatography-mass spectrometry (GC-MS) (Gilman et al.,

51  2015), but have not as yet been identified using FTIR in burning investigations. We wished to

52  determine if such species' signatures are also found sequestered in the IR spectra associated with

53  wildland fire, and are thus amenable to IR detection.  A second goal of the present study, whose

54  biomass burning results are mostly detailed in a separate manuscript, was to better understand

55  pyrolysis.  Pyrolysis is the chemical transformation of material by heat in an oxygen-free or low-

56  oxygen environment. Wildland fire consists of multiple processes: thermal decomposition

57  (pyrolysis) of solid wildland fuels into gases, tars, and char is followed by combustion (oxidation)

58  of pyrolysis products resulting in flame gases and particulate matter in the smoke. The visible

59  flame is sustained by fuel gases that are produced by pyrolysis (Ward et al., 1991). These two

60  processes (pyrolysis and combustion) are complementary given that heat released from the

61  oxidation reactions facilitates further pyrolytic reactions allowing the fire to advance.  Description

62  and measurement (by any means) of the discrete pyrolysis products adjacent to the flames of a

63  wildland fire has seldom been performed. Non-intrusive measurement of the (pyrolysis) gases in

64  the near-flame environment is desirable from both a scientific and safety perspective.

65  The major gas-phase compounds emitted from wildland fires are $H_2O$, $CO_2$, CO and $CH_4$ (Ward

66  et al., 1991), all of which are easily identified and quantified via FTIR spectroscopy. Lightweight

67  hydrocarbons, oxygenated hydrocarbons, nitrogen and sulfur species are all minor products

68  generated during burns (Yokelson et al., 1996; Lobert et al., 1991; Talbot et al., 1988). A host of

69  more complex gases which can condense to form tar are also produced by pyrolysis of wildland

70  fuels (Amini et al., 2019; Safdari et al., 2018).  In a gas-phase IR spectrum of such species,

71  however, peaks associated with the minor products are often obfuscated by more prominent

72  features, such as those from $CO_2$ or $H_2O$ and can only be recognized in the residual of a

73  multicomponent simulated fit once larger features have been removed.  Using data from a recent

74  field campaign to measure pyrolysis products carried out in a pine forest at Fort Jackson, South

75  Carolina, we have analyzed some of the IR spectra in more detail to search for the signatures of

76  compounds not found in Table 1. As a partial guide of species for which to investigate, we searched

77  for those species detected in previous thermogravimetric-FTIR (TG-FTIR) studies (Bassilakis et

78  al., 2001; Taghizadeh et al., 2015). TG-FTIR experiments, however, are typically small-scale and

79  carried out in controlled environments (in contrast to ambient conditions of prescribed burns or

80  large-scale laboratory burns) and thus represent burns with different oxidative capacities /

81  combustion efficiencies (Fang et al., 2006; Yokelson et al., 1996; Akagi et al., 2014). In this study,

82  we have chosen to examine field fire spectra for species that can be detected and quantified via IR

83  spectroscopy both to add to the list of compounds, and also to improve the characterization (and

84  ultimately the detection limits) of the other species listed in Table 1.  That is to say, fire IR spectra

85  are very complex and contain many overlapping peaks; the success of spectral analysis depends

86  both on the selected spectral region and the proper analysis of all compounds included in the fit to

87  that domain. The chemometric results become more reliable as signatures of all relevant species

88  are included in the fit.

89
90
91
92
93
94
95
96
97
98
99
100

**Table 1.** Compounds previously detected in biomass burning studies using FTIR methods (Akagi et al., 2013; Alves et al., 2010; Burling et al., 2011; Goode et al., 2000; Karl et al., 2007; Akagi et al., 2014; Burling et al., 2010; Christian et al., 2003; Christian et al., 2004; Goode et al., 1999; Selimovic et al., 2018; Stockwell et al., 2014; Yokelson et al., 1996; Yokelson et al., 1997; Yokelson et al., 2009; Hatch et al., 2017; Gilman et al., 2015).

| Compounds | | |
|---|---|---|
| Carbon monoxide (CO) | Formaldehyde (HCHO) | Nitric oxide (NO) |
| Carbon dioxide ($CO_2$) | Formic acid (HCOOH) | Nitrogen dioxide ($NO_2$) |
| Methane ($CH_4$) | Acetic acid ($CH_3COOH$) | Nitrous acid (HONO) |
| Ethane ($C_2H_6$) | Glycolaldehyde ($C_2H_4O_2$) | Ammonia ($NH_3$) |
| Ethene ($C_2H_4$) | Carbonyls as glyoxal ($C_2H_2O_2$) | Nitrous oxide ($N_2O$) |
| Acetylene ($C_2H_2$) | Methyl vinyl ether ($C_3H_6O$, MVE) | Hydrogen cyanide (HCN) |
| Propene ($C_3H_6$) | Acetone ($CH_3COCH_3$) | Peroxyacetyl nitrate ($C_2H_3NO_5$)** |
| Isobutene ($C_4H_8$) | Hydroxyacetone ($C_3H_6O_2$) | Sulfur dioxide ($SO_2$) |
| 1,3-Butadiene ($C_4H_6$) | Furan ($C_4H_4O$) | Carbonyl sulfide (OCS) |
| Isoprene ($C_5H_8$) | 2-Methylfuran ($C_5H_6O$)* | Hydrogen chloride (HCl) |
| Limonene ($C_{10}H_{16}$) | Furaldehyde ($C_4H_3OCHO$) | Ozone ($O_3$)** |
| Methanol ($CH_3OH$) | Phenol ($C_6H_5OH$) | Water ($H_2O$) |

* used in the fit, but not analyzed, ** secondary components detected downwind

## 2. EXPERIMENTAL

### 2.1 Site description and sampling device

In early May 2018, seven prescribed fires were conducted in pine forests at U.S. Army Garrison Fort Jackson, adjacent to Columbia, South Carolina, at sites not far from previous smoke emission studies (Akagi et al., 2013; Weise et al., 2015). The forest overstory was primarily longleaf pine (*Pinus palustris* Mill.) and slash pine (*Pinus elliottii* Engelm.), while sparkleberry (*Vaccinium arboreum* Marshall) dominated the understory vegetation. During each burn, pyrolyzed gases emitted at the base of the flames before ignition were collected using an extractive probe and stored in 3-liter Summa canisters. This approach was performed to selectively collect pyrolysis gases prior to the onset of combustion. Details regarding the site description and sampling apparatus will be provided in a separate paper.

## 2.2 FTIR Spectrometer

Gases were analyzed in the laboratory (on the same day or the day following the fire) using an 8-meter multipass (White) cell (Bruker Optics, A136/2-L) mounted in the sample compartment of a Bruker Tensor 37 FTIR. Ten canisters were returned from the field to the laboratory and in turn connected to the gas cell via 3/8" stainless steel tubing. The tubing and gas cell were both heated to 70 °C to prevent analyte adhesion to the inner surfaces. The White cell (White, 1942) was equipped with a pressure gauge and temperature probe, both of which were located on the gas outlet port; the thermocouple wire temperature probe extended into the White cell volume in order to more accurately measure the gas temperature. Prior to the start of the series of experiments, it was necessary to calibrate the path length of the variable path gas cell. Measurements conducted at room temperature of pure isopropyl alcohol (IPA, Sigma-Aldrich, 99.5%) at ten different pressures were collected and a Beer-Lambert Law plot was created to determine the length. The IR region from 3515 to 3290 $cm^{-1}$ was integrated (Figure 1a) using OPUS v5.5 software, and the corresponding areas plotted as a function of the IPA pressure (converted to ppm at 760 Torr) multiplied by the PNNL reference (Sharpe et al., 2004) integration area for a 1 ppm-meter IPA burden (Figure 1b). The y-intercept was set to zero. The slope is equal to the path length, which was determined to be $8.10 \pm 0.1$ m (standard error of the regression).
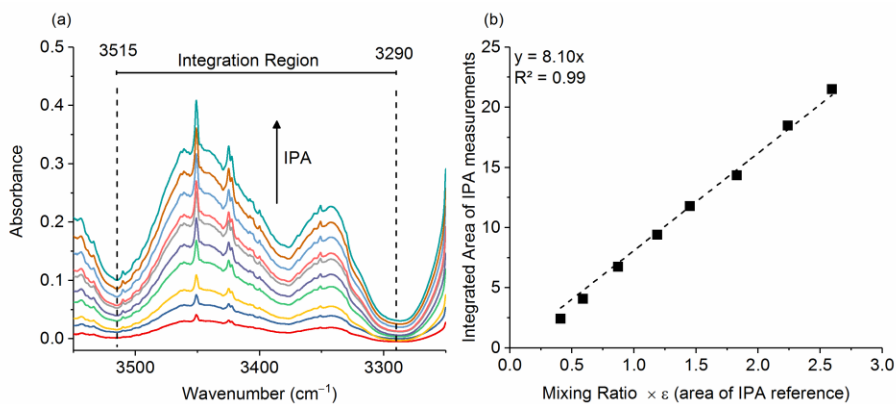
**Figure 1.** a) Multiple burden spectra of dry IPA for 10 measurements at varying pressures. The dashed lines represent the integration limits used for spectral integration. b) Calibration plot with regression line for IPA measurements. The slope of the regression is the path length in meters.

The White cell contained analyte smoke for the sample spectrum measurement but was filled with ultra-high purity nitrogen gas for the background spectrum measurement (Johnson et al., 2013). The FTIR interferometer, detector and sample compartments were purged with dry air from a dry-air generator. Inspection of a single beam background spectrum showed no evidence of CO or $CH_4$ contaminants and only negligible amounts of $H_2O$ and $CO_2$. The Tensor 37 was equipped with a globar source, a KBr beamsplitter and a broadband liquid nitrogen cooled mercury cadmium telluride (MCT) detector, providing spectral coverage from 7,500 to 500 $cm^{-1}$. The spectral resolution was 0.6 $cm^{-1}$, and a 2 mm Jacquinot aperture was used. The acquisition mode was set to double-sided, forward-backward. For the Fourier transform, data were apodized with a Blackman-Harris 3-Term function using a zerofill factor of 4 and phase corrected via the Mertz (Mertz, 1967) method.

**2.3 Quantitative Spectral Analysis**

The program used for quantitative spectral analysis was MALT5 (Griffith, 2016), and it uses both broadband reference spectra from PNNL (Sharpe et al., 2004; Johnson et al., 2009; Johnson et al., 2006; Lindenmaier et al., 2017; Profeta et al., 2011) and absorption line intensities from HITRAN (Gordon et al., 2017) [in units of $cm^{-1}/(molec \times cm^{-2})$] to iteratively fit a simulated spectrum to

160  the measured spectrum by optimizing the fit so as to minimize the mean-squared residual, i.e. the

161  difference between the measured and simulated spectra. Parameters such as path length, resolution,

162  apodization, temperature, pressure, spectral domain, target compounds / overlapping compounds

163  are all used as inputs to the spectral fit. The MALT analysis technique has previously been used

164  in both open-path and extractive FTIR systems with active sources. (Burling et al., 2010; Burling

165  et al., 2011; Akagi et al., 2013; Akagi et al., 2014). The program has also been used for ground-

166  based solar FTIR measurements (Griffith et al., 2003).

167  During the course of this study, MALT5 was used to identify multiple gas-phase species emitted

168  during the burns and quantify the gas mixing ratios via IR spectroscopy, five of them for the first

169  time. Part of the confirmation strategy is to process the experimental spectra both with and without

170  the target compound present in the fit and then to visually inspect the corresponding residuals.

171  Table 2 summarizes the IR-active vibrational mode used for each species in the spectral fit

172  (typically the species' strongest band in the longwave infrared window) along with the spectral

173  domain and a list of species with overlapping bands in that domain.

174  **Table 2.** Gas-phase species identified via FTIR, vibrational assignments (Chakraborty et al., 2016; Ghosh
175  et al., 1981; Es-Sebbar et al., 2014; Lord et al., 1952; Hamada et al., 1985; Hollenstein et al., 1971), and
176  spectral domains used for spectral fit and quantitation.

| Target compound | Vibrational bands used for analysis | Spectral region ($cm^{-1}$) | Other species fit in the same region |
|---|---|---|---|
| Naphthalene | $\nu_{46}$ at 782.3 $cm^{-1}$ | 800–760 | $C_2H_2$, $CO_2$, HCN and $H_2O$ |
| Methyl nitrite | $\nu_8$ at 841.1(*cis*) and 812.3 (*trans*) $cm^{-1}$ | 865–775 | $C_2H_2$, $CO_2$, HCN, naphthalene, $C_2H_4$, allene, and $H_2O$ |
| Allene | $\nu_{10}$ at 845.3 $cm^{-1}$ | 865–775 | $C_2H_2$, $CO_2$, HCN, naphthalene, $C_2H_4$, methyl nitrite, and $H_2O$ |
| Acrolein | $\nu_{10}$ at 1157.7 $cm^{-1}$ | 1200–1100 | Acetic acid ($CH_3COOH$), furfural ($C_4H_3OCHO$), acetaldehyde , HCOOH, $CH_4$, $C_2H_4$, and $H_2O$ |
| Acetaldehyde | $\nu_3$ at 2716.2 $cm^{-1}$ | 2800–2650 | $CH_4$, HCHO, $C_2H_2$, acrolein, and $H_2O$ |

177

178   The PNNL database provides reference spectra measured at 5, 25 and 50 °C, all of which have

179   been normalized to a number density of 296 K (~23 °C) and 1 atmosphere. While not perfectly

180   optimal, the PNNL 50 °C reference spectra were used for evaluation to best match the bandshapes

181   of the 70 °C experimental data. The fit of the 50 °C PNNL reference data to the 70 °C experimental

182   spectra is obviously less than ideal.  To correctly fit to the experimental spectra, reference data at

183   70 °C are needed, but short of this knowledge of the temperature, partition function and individual

184   line assignments are needed, and this changes for each line or set of lines for each molecule used

185   in the fit.  While MALT5 correctly accounts for gas temperature in all cases and for intensities of

186   the HITRAN line-by-line data, it cannot do so for the PNNL reference data. At higher

187   temperatures, there can be increases in population/intensity of the high-J lines with decreases for

188   the lines originating with low J values. The effect is more pronounced for smaller, more rigid

189   molecules (e.g. allene, acetaldehyde) than for the bands associated with larger, less rigid molecules

190   of low symmetry. Preliminary estimates for the quality of fit estimate errors in the 2 to 5 percent

191   range, though the value depends strongly on the species and which waveband is used for the fit.

192   **2.4 Spectral Resolution**

193   As mentioned in section 2.2, the spectral resolution was set to 0.6 cm$^{-1}$, which is the highest

194   resolution obtainable with this instrument.  There are many benefits, but also a few disadvantages

195   to using higher resolution (Herget et al., 1979). Most importantly, higher resolution allows one to

196   resolve the narrow bands of key analytes as well as interferents and discriminate the analyte signals

197   from lines or bands of interferents.  For example, the 782 cm$^{-1}$ Q-branch of naphthalene was

198   distinguished from the adjacent absorption lines of $C_2H_2$ [Naphthalene's IR bands and results are

199   discussed in greater depth in Section 3.1]. If a lower resolution were used, the deconvolution of

200   naphthalene from $C_2H_2$ would have been compromised, perhaps unfeasible. To demonstrate, one

201 of the experimental measurements collected at a resolution of 0.6 cm$^{-1}$ was deresolved to 1, 2, and

202 4 cm$^{-1}$ using a Gaussian profile as seen in Figure 2. Those spectra were processed by MALT5 to

203 check for the presence of naphthalene. Figure 2 displays the measured spectra and the scaled

204 reference spectra for $C_2H_2$ and naphthalene, and the corresponding residuals with and without

205 naphthalene included in the fit for the a) original spectrum collected at 0.6 cm$^{-1}$ and the deresolved

206 spectra at b) 1 cm$^{-1}$, c) 2 cm$^{-1}$, and d) 4 cm$^{-1}$. With the reference spectra for the original 0.6 cm$^{-1}$

207 measurement and the 1 cm$^{-1}$ deresolved spectrum (Figure 2a and b), the absorption lines for $C_2H_2$

208 and naphthalene overlap, but the 782 cm$^{-1}$ feature from naphthalene is still slightly visible in the

209 original spectra. The naphthalene peak appears clearly in the residuals when it is not included in

210 the fitting process, but is removed from the residual when naphthalene is included in the fit

211 (discussed further below). As the resolution is further reduced (Figures 2c and 2d), however, the

212 features broaden, and the distinction of the naphthalene peak from $C_2H_2$ and other minor

213 components (i.e. $CO_2$, HCN, $H_2O$, spectra not shown) is compromised. The specificity between

214 compounds is lost and confidence in the identification/quantification of the target species,

215 particularly for the weaker absorbers, diminishes as the resolution decreases. The well-known

216 benefits of using a lower resolution are that spectra can be acquired more quickly at an improved

217 signal-to-noise ratio. For the present measurements, 0.6 cm$^{-1}$ was deemed an appropriate

218 resolution.
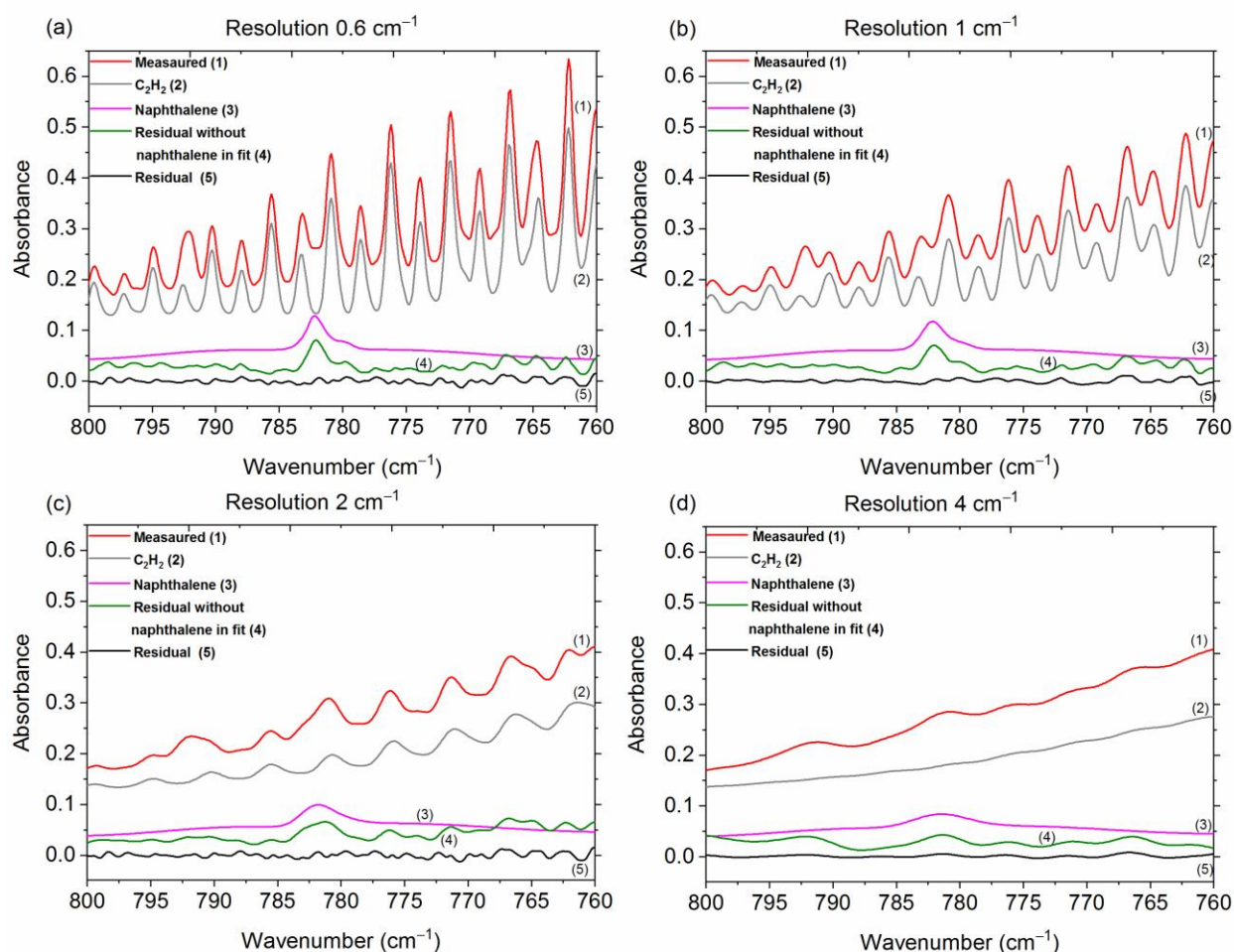
**Figure 2.** Measured and scaled reference spectra for $C_2H_2$ and naphthalene, and corresponding residuals with and without naphthalene included in the fit for the a) original spectrum collected at 0.6 $cm^{-1}$ and the deresolved spectra at b) 1 $cm^{-1}$, c) 2 $cm^{-1}$, and d) 4 $cm^{-1}$. The reference spectra for $CO_2$, HCN and $H_2O$ are not shown (HCN was not included in fit when the resolution was 4 $cm^{-1}$; for resolutions 1, 2 and 4 $cm^{-1}$, $H_2O$ was not included in the fit when naphthalene was removed from the fit). Spectra are offset for clarity.

## 2.5 Signal-to-Residual Detection Limits

In IR spectroscopy, detection limits often represent the minimum amount of analyte that may be detected and are often reported as two to three times the noise level (Griffith et al., 2006). The detection limit values presented in this paper are not minimal signal-to-noise limits in the sense of a minimal spectral signal against a background of purely stochastic noise sources. In such cases, the noise sources are typically of comparable or higher frequencies than the signal (Johnson et al.,

11

232 1991). Rather, the current limits represent average detection limits for a spectral residual derived

233 from a convoluted spectrum arising from a gas mixture of differing and fluctuating chemical

234 composition. The residuals are due to a least-squares fit of (fluctuations in) many complex features

235 arising from numerous chemicals. That is to say, the residual is not due to just random instrumental

236 noise but due to spectral features that can arise in the spectra, e.g. imperfectly subtracted features

237 from strong absorbers or unidentified absorbers. For that reason, we report signal-to-residual

238 rather than signal-to-noise detection limits. The detection limits for each compound in this study

239 were thus derived using a value of three times the root-mean-square (RMS) value of the residual

240 calculated over the corresponding frequency range (e.g. 800–760 $cm^{-1}$ was used for naphthalene).

241 The peak-to-peak noise is more sensitive to fluctuations in the fit with levels typically 4 to 5× the

242 RMS noise (Griffith et al., 2006). For the present data, however, the peak-to-peak values ranged

243 from 5 to 10× the RMS noise, thus suggesting the peak-peak values tend to overstate the tractable

244 noise level, i.e. understate the detection limit. The reported detection limits are thus presumably

245 higher than what would be estimated with an FTIR in clean air conditions (i.e. only the analyte

246 and dry air). Based on experience, the limits are typically far higher than what can be obtained

247 with IR laser sensors where the intrinsically narrow laser linewidths allow for the probing of

248 individual rotational-vibrational lines without drawing in overlapping spectral lines to a congested

249 spectral fit (Taubman et al., 2004; Phillips et al., 2014; Wagner et al., 2011). While typically far

250 more sensitive, such laser measurements can only analyze for one or a few species at a time, as

251 opposed to the 30+ species seen by the broadband FTIR measurements.

## 3. RESULTS AND DISCUSSION

253 When modeling the burning process (Byram, 1959), complete combustion of 1 kg dry wood

254 produces 1.82 kg $CO_2$ and 0.32 kg $H_2O$ for a total mass of products of 2.14 kg. Incomplete

255 combustion will yield additional products and less $CO_2$ and $H_2O$ while combustion of wet fuels

256 (Byram, 1959) increases the amount of $H_2O$ released. For infrared analysis of such smoke, much

257 of the challenge arises due not only to the large mole fractions of $H_2O$ and $CO_2$, but to the fact that

258 both $H_2O$ vapor and $CO_2$ have strong features in the mid-IR that can clutter the spectrum rendering

259 certain spectral regions unusable. For burning and other atmospheric studies, ideal compounds for

260 detection via IR spectroscopy will thus have strong absorption coefficients that do not overlap with

261 the fundamental bands of $H_2O$ or $CO_2$, i.e. are in a spectral window or microwindow (Griffith,

262 1996; Esler et al., 2000; Smith et al., 2011) free of strong interferences. Here, we consider five

263 such compounds emitted during this prescribed burn, but which had heretofore not been reported

264 as being detected by FTIR. Table 3 presents the range of measured mixing ratios for the target

265 compounds along with averaged detection limits for 10 measurements collected during the

266 prescribed burns. Individual compounds are discussed in turn regarding their formation

267 mechanism(s) as well as their detectable IR features and spectral confirmation for this study.

268 Lastly, the results are briefly compared with literature values using emission ratios (mixing ratios

269 of analyte to excess CO).

270 **Table 3.** Calculated mixing ratios for ten canister FTIR measurements along with average estimated
271 residual detection limits for the target compounds derived using 3 times the root-mean-square of the
272 residual in very congested spectra. Error bars represent standard deviation ($1\sigma$) from the mean.

| Target compound | Calculated mixing ratios (ppm) | | | Averaged residual detection limit (ppm) using root-mean-square (RMS) value of the residual |
|---|---|---|---|---|
| | Min | Max | Average | |
| Naphthalene* | 1.4 | 19.9 | $8.5 \pm 2.1$ | $1.9 \pm 0.5$ |
| Methyl nitrite* | 2.3 | 21.0 | $8.7 \pm 2.4$ | $2.2 \pm 0.4$ |
| Allene | 2.2 | 37.8 | $13.1 \pm 3.6$ | $3.0 \pm 0.6$ |
| Acrolein | 14.7 | 125.7 | $43 \pm 12$ | $6.1 \pm 1.5$ |
| Acetaldehyde | 34.5 | 264.8 | $103 \pm 27$ | $11.7 \pm 3.2$ |

273 *One measurement was below the detection limit.
274

**3.1 Naphthalene**

Naphthalene ($C_{10}H_8$) is a polycyclic aromatic hydrocarbon (PAH) that is emitted from certain industrial processes as well as from the combustion of gasoline and oil (Jia et al., 2010). It is a condensable hydrocarbon also generated by biomass pyrolysis (Liu et al., 2017). There are a number of pyrolysis formation routes (Williams et al., 1999; Liu et al., 2017; Lu et al., 2004; Fairburn et al., 1990; Richter et al., 2000). One proposed mechanism is the generation of single ring aromatic compounds such as benzene, toluene and styrene via Diels-Alder reaction of alkenes; the single ring aromatic compound then combines with alkenes to form double-ring PAHs, such as naphthalene (Fairburn et al., 1990). Naphthalene may even undergo subsequent reactions to form still larger polyaromatics (Fairburn et al., 1990; Richter et al., 2000). Naphthalene has been detected (via GC-MS) in tars that were condensed from gas-phase pyrolysis products of both live and dead southeastern fuels, such as live oak (*Quercus virginiana*) and swamp bay (*Persea palustris*) (Safdari et al., 2018). It has also been detected (Koss et al., 2018; Hosseini et al., 2014; Aurell et al., 2017) in the gas-phase in laboratory burning experiments. The detection of gas-phase naphthalene from wildland fire emissions is thus not surprising, but this is the first report of its identification via IR spectroscopy. The best spectral feature for identification and quantification is the $\nu_{46}$ IR mode near 782.3 $cm^{-1}$, which corresponds to the H–C–C out-of-plane bend (Chakraborty et al., 2016). There are other bands at 3067.7 and 3058.0 $cm^{-1}$ previously assigned to $\nu_{29}$ and $\nu_{17}$, respectively (Chakraborty et al., 2016). Both of these modes have smaller absorption coefficients as compared to $\nu_{46}$, however, and are located in the C–H stretching region, which is common to nearly all hydrocarbons and thus provides less specificity.

Figure 3 shows a prescribed burn spectrum in the region from 800 to 760 $cm^{-1}$. The primary spectral signatures in this plot are those of R-branch rotational-vibrational lines associated with

14

298     the $\nu_5$ fundamental of $C_2H_2$ (Kabbadj et al., 1991), but there are also absorptions due to $CO_2$, HCN,

299     $H_2O$ (individual spectral contributions not shown) and naphthalene. When all of the spectral

300     components except for naphthalene are included in the fitting process, the residual (green trace,

301     #4) displays a prominent feature at 782.3 $cm^{-1}$, which we ascribe to naphthalene. When

302     naphthalene is included in the fit, the feature in question is not seen as demonstrated by the black

303     trace (#5) of Figure 3. Including naphthalene in the analysis clearly improves the fit, which

304     consequently improves the derived values for the other species. This observation is consistent in

305     the spectral analyses for all target compounds discussed below.



306
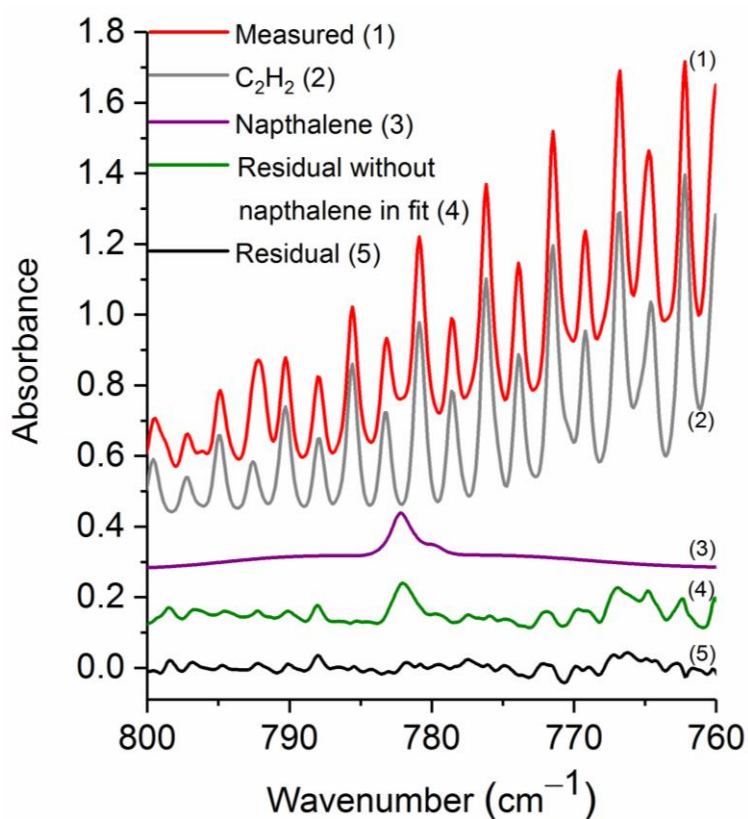
**Figure 3.** Measured spectrum, scaled reference spectra for $C_2H_2$ and naphthalene, and residuals with and
without naphthalene included in the fit. For clarity, the spectral contributions for $CO_2$, HCN, and $H_2O$ are
not shown. All spectra are at 0.6 $cm^{-1}$ resolution and have been offset. The calculated mixing ratio of
naphthalene in this measured spectrum is 16.4 ppm.

311

312

15

313 Table 3 displays the range of measured mixing ratios for naphthalene along with averaged

314 detection limits for the 10 measurements. In the measurements, naphthalene's mixing ratios

315 ranged from 1.4 to 19.9 ppm, and the averaged RMS-derived detection limit was $1.6 \pm 0.5$ ppm;

316 different detection limits were observed for each spectrum. One of the measurements had a mixing

317 ratio of 2.9 ppm, yet its corresponding RMS-derived detection limit was 3.7 ppm, and is thus below

318 the estimated detection limit.

319 **3.2 Methyl Nitrite**

320 A second compound detected for the first time in wildland fire IR spectra was methyl nitrite

321 ($CH_3ON=O$). Methyl nitrite has previously been observed in aged cigarette smoke (Schmeltz et

322 al., 1977) and the exhaust of engines fueled by methanol–diesel blends (Jonsson et al., 1982). It

323 has also been observed as a minor product for the thermal decomposition of both nitrate esters

324 (Boschan et al., 1955) and isopropyl nitrate at low temperatures and pressures (Griffiths et al.,

325 1975). Methyl nitrite has moreover been detected in wildland fire emissions by GC-MS (Gilman

326 et al., 2015). Other nitrogen-containing organic compounds such as acetonitrile ($CH_3CN$) emitted

327 from burns have been previously correlated to the fuel nitrogen content. However, methyl nitrite

328 [and another oxygenated nitrogen organic compound, isocyanic acid (HNCO)] did not show any

329 significant dependency on fuel N-content (Coggon et al., 2016). It has been suggested that methyl

330 nitrite is not only a minor direct product of combustion (Finlayson-Pitts et al., 1992), but in

331 addition is generated *in situ* by the secondary reaction of methanol ($CH_3OH$) with nitrogen dioxide

332 ($NO_2$).

333 We also note that methyl nitrite is an oxidizing agent and is used as a rocket propellant. It is thus

334 plausible that the methyl nitrite detected in the present study was not a product of the fire, but

335 emanated from munitions used in training at Ft. Jackson. However, while the records of the

336    munitions used at all base sites were not complete, a survey of these records did not indicate the

337    use of methyl nitrite in any munitions at the Ft. Jackson plots where the present burn samples were

338    collected.

339    With regards to the IR spectra, methyl nitrite exists in equilibrium as a mixture of two conformers-

340    *cis* and *trans*; at room temperature (25 °C) it is estimated as 58% *cis* and 42% *trans* (Bodenbinder

341    et al., 1994). The PNNL reference spectrum for methyl nitrite was created using a nascent mixture

342    of *cis* and *trans*, and the single spectrum contains features from both conformers (Sharpe et al.,

343    2004). We were able to use the same band associated with both conformers, namely the $\nu_8$ band,

344    which is at 841.1 $cm^{-1}$ for the *cis* conformer and at 812.4 $cm^{-1}$ for the *trans* conformer (Ghosh et

345    al., 1981). The $\nu_8$ mode is associated with the N–O stretch and is very strong for both conformers

346    (Ghosh et al., 1981). We note that methyl nitrite also has very strong bands at 627.8 $cm^{-1}$ (*cis*) for

347    $\nu_9$ ONO bending, as well as at 1620.1 $cm^{-1}$ (*cis*) and 1677.4 $cm^{-1}$ (*trans*) due to the $\nu_3$ N=O stretch

348    (Ghosh et al., 1981). These bands, however, are of lesser utility for IR detection: The $\nu_9$ peak is

349    masked by $CO_2$ bending mode lines, and the $\nu_3$ peak is obfuscated by the $H_2O$ bending mode lines.

350    The spectral region used for evaluation was 865–775 $cm^{-1}$, which contains the $\nu_8$ band for both the

351    *cis* and *trans* conformers (Ghosh et al., 1981).  Figure 4 shows the experimental spectrum from

352    the prescribed burn along with scaled reference spectra for the two major compounds used in the

353    fit: $C_2H_2$ and methyl nitrite. While important, other minor compounds, such as $CO_2$, HCN,

354    naphthalene, $C_2H_4$, allene and $H_2O$, were also included in the analysis, but their spectral

355    contributions are not plotted. Additionally, Figure 4 displays the residuals both when methyl nitrite

356    was included in the fitting process and when it was excluded. Upon inspection of the residual

357    spectrum where it was excluded (green trace, #4), it is clear that both the *cis* and *trans* features

358    from $\nu_8$ are present, and this confirms methyl nitrite in the pyrolysis smoke.

17
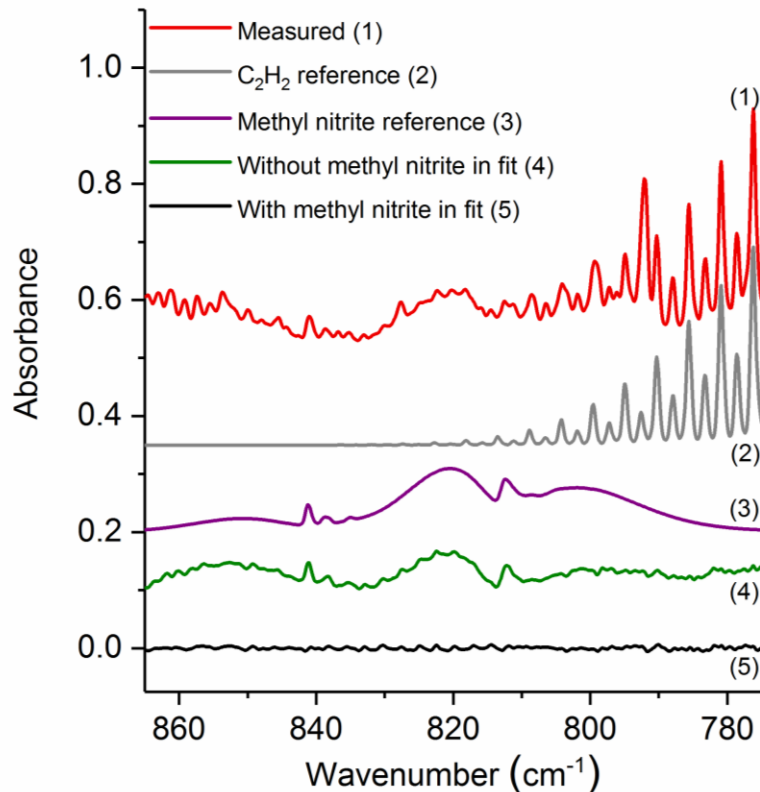
**Figure 4.** Measured experimental spectrum and the individual spectral contributions for the major components ($C_2H_2$ and methyl nitrite) and residuals with and without methyl nitrite included in the fit. For clarity, the spectral contributions for $CO_2$, HCN, naphthalene, $C_2H_4$, allene, and $H_2O$ are not shown. All spectra are at 0.6 cm$^{-1}$ resolution and have been offset for clarity. The calculated mixing ratio of methyl nitrite in this measured spectrum is 21.0 ppm.

The mixing ratio and RMS-derived detection limit for methyl nitrite for the displayed experimental spectrum in Figure 4 are 21.0 ppm and 1.4 ppm, respectively. The range for mixing ratios and averaged detection limits for methyl nitrite are summarized in Table 3. Methyl nitrite was detected with confidence in 9 of the 10 measurements; only one of the measurements was below the RMS-derived detection limit.

**3.3 Allene**

Allene (1,2-propadiene, $CH_2=C=CH_2$) is of high symmetry ($D_{2d}$) and has the two methylene groups with their H–C–H planes at right angles to each other (Lord et al., 1952). The compound has previously been detected in biomass burning grab samples using GC (Akagi et al., 2013).

18

375     Allene is a proposed precursor in the burning process that contributes to the formation of both

376     aromatic compounds and soot (Frenklach et al., 1983; Frenklach et al., 1988). Lifshitz et al. have

377     observed (at temperatures ranging from 757–847 °C) that the structural isomerization of allene and

378     propyne ($CH_2=C=CH_2 \leftrightarrow CH_3-C\equiv CH$) will take place via a unimolecular reaction faster than the

379     decomposition reaction (Lifshitz et al., 1975). Additionally, these same authors investigated the

380     pyrolysis of allene and propyne and observed that $C_2H_4$ was generated from allene while $CH_4$ and

381     $C_2H_2$ were mainly formed from propyne (Lifshitz et al., 1976). Unfortunately, the strongest IR

382     band for propyne (near $634 \text{ cm}^{-1}$) is obscured by $CO_2$ bending mode lines. Due to the interferences

383     we cannot with confidence identify propyne in the measurements; we can, however, detect allene.

384     In the mid-IR, allene has several strong rotational-vibrational lines near $845 \text{ cm}^{-1}$ associated with

385     the sub-bands of the perpendicular band $\nu_{10}$, which is due to $CH_2$ rocking (Lord et al., 1952).

386     Additionally, allene has a moderately strong band at $1958.6 \text{ cm}^{-1}$ due to the $\nu_6$ C–C stretching

387     (Lord et al., 1952). However, the $\nu_6$ band is not useful for detection due to interference from the

388     $H_2O$ bending mode lines.
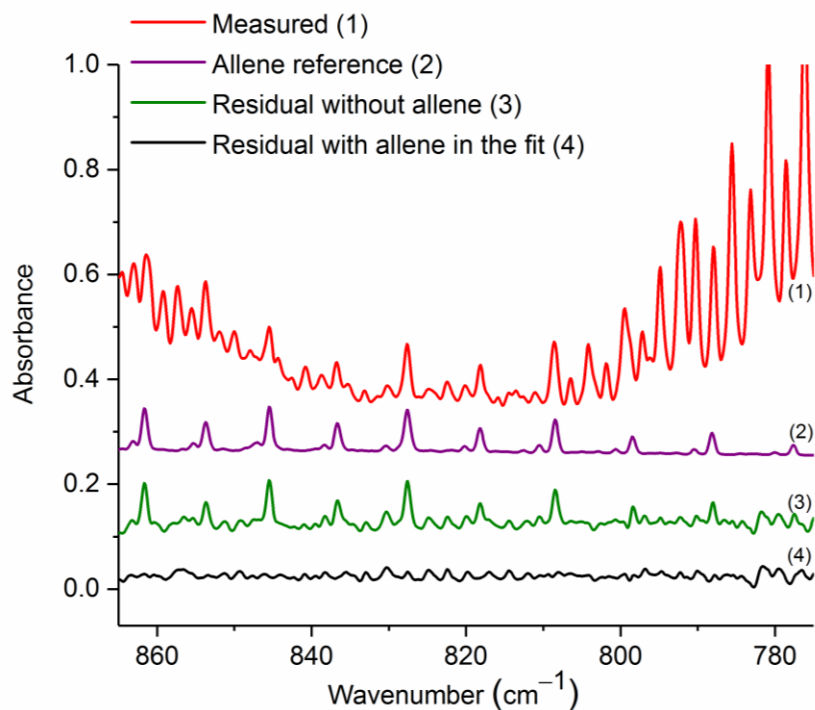
**Figure 5.** Measured absorbance spectrum and residual with and without allene included in the fit, along with the scaled reference spectrum for allene. For clarity, the spectral contributions for $C_2H_2$, $CO_2$, HCN, naphthalene, $C_2H_4$, methyl nitrite, and $H_2O$ are not shown. All spectra are at 0.6 cm$^{-1}$ resolution and have been offset for clarity. The calculated mixing ratio of allene in this measured spectrum is 37.8 ppm.

Figure 5 shows the measured absorbance spectrum, scaled allene reference spectrum and the associated residual with and without allene included in the fit. The absorption lines associated with allene are clearly seen in the resulting spectrum when allene is not included in the fit (green trace, #3), thus confirming that allene is one of the primary components contributing to the features in this spectral domain. For the experimental spectrum displayed in Figure 5, the calculated mixing ratio for allene is 37.8 ppm, and the RMS-derived detection limit is 5.4 ppm.

**3.4 Acrolein and Acetaldehyde**

The two aldehydes, acrolein ($CH_2$=CHCHO) and acetaldehyde ($CH_3$CHO), have also been identified for the first time in burning IR spectra. It has been proposed that both acrolein and

20

405 acetaldehyde are formed from the pyrolysis of cellulose (a major constituent of biomass) via the

406 intermediate glycerol, which is a moiety in the structure of levoglucosan, a known pyrolysis

407 product of cellulose (Stein et al., 1983). Stein et al. observed that acrolein, acetaldehyde and CO

408 were the initial decomposition products from the pyrolysis of glycerol (Stein et al., 1983). Both

409 of these compounds have been detected in previous wildland fires studies via methods such as GC

410 (Akagi et al., 2013) and PTR-ToF (Koss et al., 2018; Brilli et al., 2014), but have not yet been

411 identified via IR.

412 Acrolein, the simplest unsaturated carbonyl, exists in two forms, *s-cis* and *s-trans*, with *s-trans*

413 being the more stable, and consequently the more abundant conformer (Wagner et al., 1957). It

414 has been estimated that the fractions of *s-cis* and *s-trans* are about 4 and 96% at 20 °C, and 7 and

415 93% at 100 °C, respectively (Alves et al., 1971). The largest IR feature for acrolein is the $\nu_5$ C=O

416 stretch (Hamada et al., 1985) at 1724.1 $cm^{-1}$, but this band is heavily overlapped by water lines.

417 There is also the $\nu_{16}$ band (Hamada et al., 1985) at 958.8 $cm^{-1}$, but this feature overlaps with

418 multiple other strongly absorbing compounds, such as $C_2H_4$. We have therefore focused acrolein's

419 analysis using the $\nu_{10}$ band (C–C stretch) (Hamada et al., 1985) at 1157.7 $cm^{-1}$.

420 Figure 6 displays a very congested biomass burning spectrum with individual contributions for

421 several species included in the fit [contributions for furfural ($C_4H_3OCHO$), acetaldehyde, $CH_4$, and

422 $C_2H_4$ are included, but not plotted] as well as the residual with and without acrolein included in

423 the fitting process. When acrolein is not included in the fit, features (both near 1168 and at 1157.7

424 $cm^{-1}$) that resemble acrolein are observed in the residual spectrum as seen in the green trace in

425 Figure 6. When acrolein is included in the fit, the features in question are not observed. For

426 acrolein, no mixing ratios were observed below the RMS-derived detection limits.
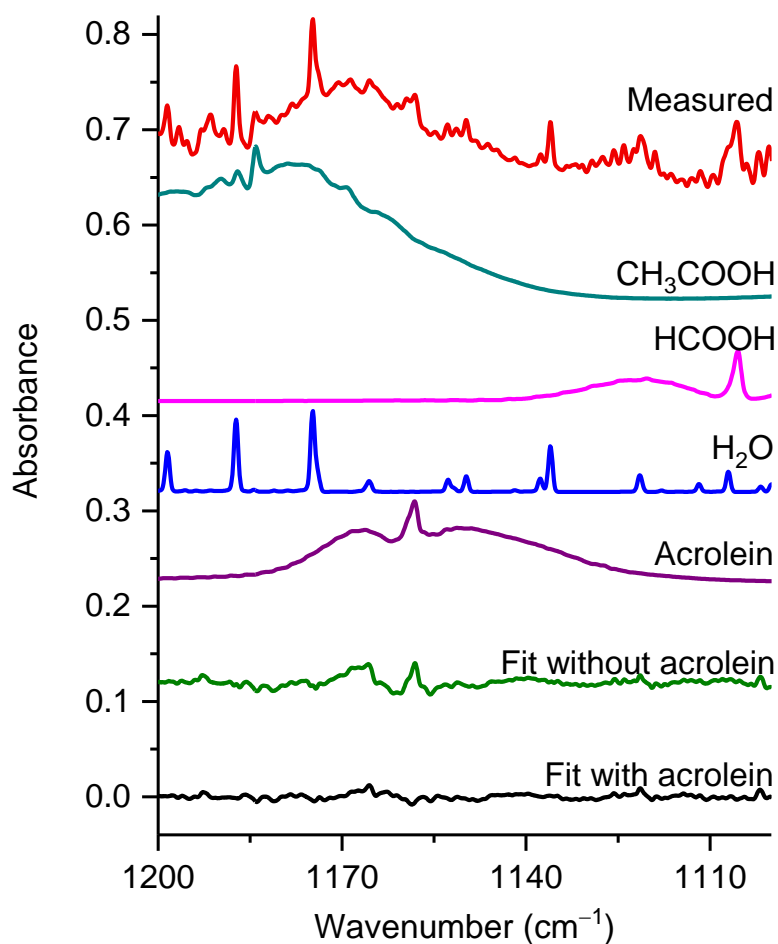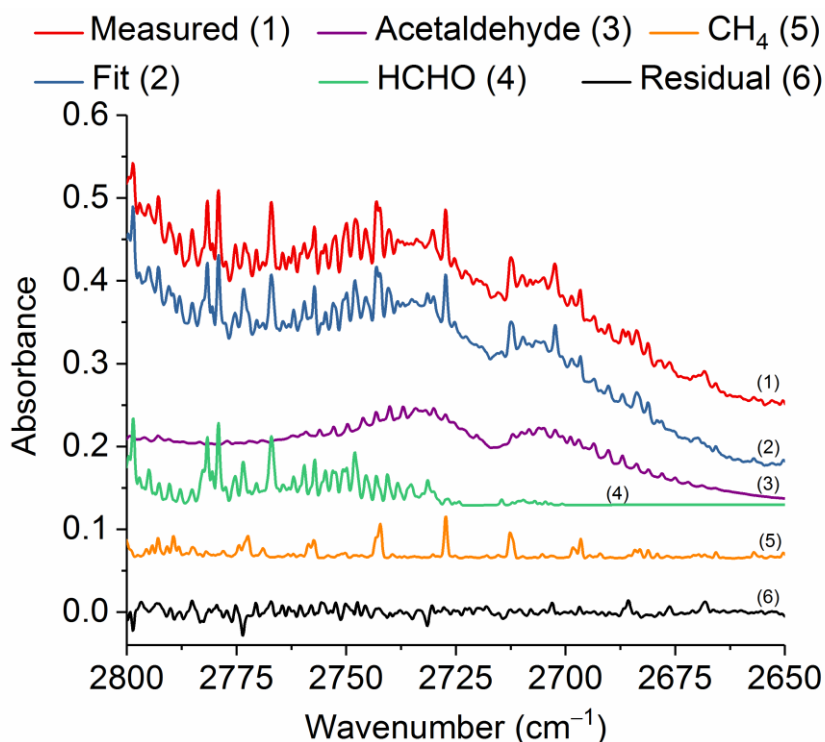
**Figure 6.** Measured spectrum and the individual spectral contributions for the major components and associated residual with and without acrolein included in the fit. For clarity, the spectral contributions for furfural ($C_4H_3OCHO$), acetaldehyde, $CH_4$, and $C_2H_4$ are not shown. All spectra are at 0.6 cm$^{-1}$ resolution and have been offset for clarity. The calculated mixing ratio of acrolein in this measured spectrum is 99.9 ppm.

Similar to acrolein, acetaldehyde has its strongest IR feature due to the C=O stretch (Hollenstein et al., 1971), with $\nu_4$ found at 1746.1 cm$^{-1}$. Again, due to the presence of water lines in the spectrum, this feature is not practical for detection. The aldehyde $\nu_3$ C–H stretching band (Hollenstein et al., 1971) at 2716.2 cm$^{-1}$ was instead used for analysis. Figure 7 shows the measured and fitted spectra as well as spectral contributions from the major individual components

439    used to calculate the fitted spectrum and the corresponding residual.  Other minor components,

440    such as acrolein, $C_2H_2$ and $H_2O$, were also included in the fit, but their reference spectra are not

441    displayed in Figure 7. The spectral profile of acetaldehyde with its P and R branches of $v_3$ is easily

442    discernable even before deconvolution of the measured spectrum. Similar to acrolein, all of the

443    mixing ratios for acetaldehyde were above the RMS-derived detection limit.

444



445
446    **Figure 7.** Measured and fitted spectra as well as the individual components (for clarity, the spectral
447    contributions for acrolein, $C_2H_2$, $H_2O$ are not shown) and associated residual in the spectral region 2800–
448    2650 cm$^{-1}$. All spectra are at 0.6 cm$^{-1}$ resolution and have been offset for clarity. The calculated mixing
449    ratio of acetaldehyde in this measured spectrum is 252.8 ppm.
450

451    **3.5 Comparison to Other Measurements**

452    Preliminary emission ratios (relative to carbon monoxide) for the five new reported compounds

453    are compared to those presented in previous wildland burning investigations. An emission ratio is

454    a standard metric used in fire emission measurements and is defined as the change in the mixing

455    ratio of the target compound relative to the change in mixing ratio of the reference species,

456 generally either carbon monoxide or carbon dioxide (Urbanski et al., 2008). Here, carbon

457 monoxide is used as the reference species since the present study focuses on pyrolysis, and prior

458 fire studies generally provide emission ratios relative to carbon monoxide, which makes it a

459 convenient quantity for comparison. Table 4 displays the average emission ratios and the standard

460 deviations ($1\sigma$) for this study as well as emission ratios reported by Koss et al. (2018), Ferek et al.

461 (1998), Brilli et al. (2014), and Gilman et al. (2015). As shown in the table, there is considerable

462 variation between the studies due to multiple factors such as different fuel types, analytical

463 methods, sampling approaches and experimental conditions. For example, the study by Ferek et

464 al. (1998) focused on collection of airborne samples, while Brilli et al. (2014) measured gases

465 under nocturnal conditions using a ground-based system. Inspection of the table shows that the

466 measured emission ratio values are not unprecedented, and in most cases are within range of

467 previous measurements. Because they have the same molar mass, the mass spectrometric

468 techniques in some cases cannot distinguish allene from propyne. There are of course advantages

469 and disadvantages for the various measurement techniques typically used in biomass burning

470 investigations. For a detailed summary of instrumental methods (including species measured, time

471 resolution and detection limits), the reader is referred to Table 1 found in Koss et al. (2018). The

472 FTIR technique presented in that table is open-path (OP-FTIR), which has a lower (better)

473 detection limit (typically on the order of 10s of ppb) as compared to the extractive method used in

474 the present study (low ppm, see Table 3). It should be acknowledged that the target compounds

475 and spectral analysis methods of this study are also fully applicable to both infrared laser systems

476 and OP-FTIR systems.

477

478

479 **Table 4.** Emission ratios relative to CO and standard deviations (1σ) for the present study and for three
480 other previously published biomass burning studies.

| Target compounds | Present average emission ratios to CO (ppb/ppm) | Koss et al. (2018) fire-integrated emission ratio to CO (ppb/ppm) | Ferek et al. (1998) emission ratio to CO (ppb/ppm) | Brilli et al. (2014) emission ratios to CO (ppb/ppm) | Gilman et al. (2015) discrete emission ratios to CO (ppb/ppm) | | |
|---|---|---|---|---|---|---|---|
| | | | | | South-western fuels | South-eastern fuels | Northern fuels |
| Method | FTIR | PTR-ToF-MS | GC-FID* | PTR-ToF-MS | GC-MS | GC-MS | GC-MS |
| Naphthalene | 0.79 ± 0.47 | 0.20 ± 0.16 | n/a | n/a | 0.0070 ± 0.0048 | 0.0040 ± 0.0050 | 0.022 ± 0.012 |
| Methyl nitrite | 0.94 ± 0.85 | n/a | n/a | n/a | 0.9 ± 1.1 | 0.52 ± 0.51 | 0.76 ± 0.90 |
| Acrolein | 4.0 ± 1.8 | 5.4 ± 3.0 | n/a | 3.14 ± 0.12 | 0.82 ± 0.68 | 1.31 ± 0.88 | 3.5 ± 1.7 |
| Acetaldehyde | 9.4 ± 3.6 | 7.4 ± 5.2 | n/a | 37.3 ± 1.4 | 1.6 ± 1.2 | 2.8 ± 1.8 | 5.5 ± 3.6 |
| Allene (Propadiene)** | 1.05 ± 0.24 | n/a | 0.1 ± 0.1 | 8.73 ± 0.28 | n/a | n/a | n/a |

481 *GC-FID is gas chromatography with flame ionization detector
482 **Brilli et al. (2014) use both 1-propyne and propadiene to represent $C_3H_4$. Gilman et al. (2015) report emission
483 ratios for propyne, but not allene.
484

## 4. SUMMARY

486 Gas-phase compounds with appreciable band intensities and appreciable concentrations can be

487 both identified and quantified using IR spectroscopy. We have used such spectral information for

488 seminal IR detection of five compounds generated during prescribed forest fire burns. Deriving

489 the mixing ratios from the congested spectra obtained from wildland smoke samples is more

490 challenging due to the multiple overlapping spectral features: Sophisticated software and analysis

491 are required in carefully selected spectral windows. We have reported first IR detections of five

492 molecules that had previously not been observed by FTIR in ambient measurements of wildland

493 emissions. Most of the compounds (excluding acetaldehyde), had their primary features become

494 apparent only after the larger spectral features had been fitted and subtracted.

495

496

497

## 5. REFERENCES

Akagi, S. K., Yokelson, R. J., Wiedinmyer, C., Alvarado, M. J., Reid, J. S., Karl, T., Crounse, J. D., and Wennberg, P. O.: Emission factors for open and domestic biomass burning for use in atmospheric models, Atmos. Chem. Phys., 11, 4039-4072, 2011.

Akagi, S. K., Yokelson, R. J., Burling, I. R., Meinardi, S., Simpson, I., Blake, D. R., McMeeking, G. R., Sullivan, A., Lee, T., Kreidenweis, S., Urbanski, S., Reardon, J., Griffith, D. W. T., Johnson, T. J., and Weise, D. R.: Measurements of reactive trace gases and variable $O_3$ formation rates in some South Carolina biomass burning plumes, Atmos. Chem. Phys., 13, 1141-1165, 2013.

Akagi, S. K., Burling, I. R., Mendoza, A., Johnson, T. J., Cameron, M., Griffith, D. W. T., Paton-Walsh, C., Weise, D. R., Reardon, J., and Yokelson, R. J.: Field measurements of trace gases emitted by prescribed fires in southeastern US pine forests using an open-path FTIR system, Atmos. Chem. Phys., 14, 199-215, 2014.

Alves, A. C. P., Christoffersen, J., and Hollas, J. M.: Near ultra-violet spectra of the *s-trans* and a second rotamer of acrolein vapour, Mol. Phys., 20, 625-644, 1971.

Alves, C. A., Gonçalves, C., Pio, C. A., Mirante, F., Caseiro, A., Tarelho, L., Freitas, M. C., and Viegas, D. X.: Smoke emissions from biomass burning in a Mediterranean shrubland, Atmos. Environ., 44, 3024-3033, 2010.

Amini, E., Safdari, M.-S., DeYoung, J. T., Weise, D. R., and Fletcher, T. H.: Characterization of pyrolysis products from slow pyrolysis of live and dead vegetation native to the southern United States, Fuel, 235, 1475-1491, https://doi.org/10.1016/j.fuel.2018.08.112, 2019.

Andreae, M. O.: Biomass burning: its history, use, and distribution and its impact, Global Biomass Burning: Atmospheric, Climatic, and Biospheric Implications, 1991.

532    Andreae, M. O., and Merlet, P.: Emission of trace gases and aerosols from biomass burning, Global
533        Biogeochem. Cycles, 15, 955-966, 2001.
534    Aurell, J., Gullett, B. K., Tabor, D., and Yonker, N.: Emissions from prescribed burning of timber slash
535        piles in Oregon, Atmos. Environ., 150, 395-406, 2017.
536    Bassilakis, R., Carangelo, R. M., and Wojtowicz, M. A.: TG-FTIR analysis of biomass pyrolysis, Fuel,
537        80, 1765-1786, 2001.
538    Bodenbinder, M., Ulic, S. E., and Willner, H.: A gas-phase and matrix isolation study of the equilibrium
539        $CH_3ONO$ (cis) $\rightleftarrows$ $CH_3ONO$ (trans) by FTIR spectroscopy, J. Phys. Chem., 98, 6441-6444, 1994.
540    Boschan, R., Merrow, R. T., and van Dolah, R. W.: The chemistry of nitrate esters, Chem. Rev., 55, 485-
541        510, 1955.
542    Brilli, F., Gioli, B., Ciccioli, P., Zona, D., Loreto, F., Janssens, I. A., and Ceulemans, R.: Proton transfer
543        reaction time-of-flight mass spectrometric (PTR-TOF-MS) determination of volatile organic
544        compounds (VOCs) emitted from a biomass fire developed under stable nocturnal conditions, Atmos.
545        Environ., 97, 54-67, 2014.
546    Burling, I. R., Yokelson, R. J., Griffith, D. W. T., Johnson, T. J., Veres, P., Roberts, J. M., Warneke, C.,
547        Urbanski, S. P., Reardon, J., Weise, D. R., Hao, W. M., and de Gouw, J.: Laboratory measurements of
548        trace gas emissions from biomass burning of fuel types from the southeastern and southwestern United
549        States, Atmos. Chem. Phys., 10, 11115-11130, 2010.
550    Burling, I. R., Yokelson, R. J., Akagi, S. K., Urbanski, S. P., Wold, C. E., Griffith, D. W. T., Johnson, T.
551        J., Reardon, J., and Weise, D. R.: Airborne and ground-based measurements of the trace gases and
552        particles emitted by prescribed fires in the United States, Atmos. Chem. Phys., 11, 12197-12216, 2011.
553    Byram, G. M.: Combustion of forest fuels. In 'Forest fire: control and use'. (Ed. KP Davis) pp. 61–89,
554        McGraw-Hill: New York, 1959.
555    Chakraborty, S., Banik, S., and Das, P. K.: Anharmonicity in the vibrational spectra of naphthalene and
556        naphthalene-$d_8$: Experiment and theory, J. Phys. Chem. A, 120, 9707-9718, 2016.
557    Christian, T. J., Kleiss, B., Yokelson, R. J., Holzinger, R., Crutzen, P. J., Hao, W. M., Saharjo, B. H., and
558        Ward, D. E.: Comprehensive laboratory measurements of biomass-burning emissions: 1. Emissions
559        from Indonesian, African, and other fuels, J. Geophys. Res. Atmos., 108, 2003.
560    Christian, T. J., Kleiss, B., Yokelson, R. J., Holzinger, R., Crutzen, P. J., Hao, W. M., Shirai, T., and
561        Blake, D. R.: Comprehensive laboratory measurements of biomass-burning emissions: 2. First
562        intercomparison of open-path FTIR, PTR-MS, and GC-MS/FID/ECD, J. Geophys. Res. Atmos., 109,
563        2004.
564    Coggon, M. M., Veres, P. R., Yuan, B., Koss, A., Warneke, C., Gilman, J. B., Lerner, B. M., Peischl, J.,
565        Aikin, K. C., Stockwell, C. E., Hatch, L. E., Ryerson, T. B., Roberts, J. M., Yokelson, R. J., and de
566        Gouw, J. A.: Emissions of nitrogen-containing organic compounds from the burning of herbaceous
567        and arboraceous biomass: Fuel composition dependence and the variability of commonly used nitrile
568        tracers, Geophys. Res. Lett., 43, 9903-9912, 2016.
569    Crutzen, P. J., Heidt, L. E., Krasnec, J. P., Pollock, W. H., and Seiler, W.: Biomass burning as a source of
570        atmospheric gases CO, $H_2$, $N_2O$, NO, $CH_3Cl$ and COS, Nature, 282, 253, 1979.
571    Crutzen, P. J., and Andreae, M. O.: Biomass burning in the tropics: Impact on atmospheric chemistry and
572        biogeochemical cycles, Science, 250, 1669-1678, 1990.
573    Es-Sebbar, E., Jolly, A., Benilan, Y., and Farooq, A.: Quantitative mid-infrared spectra of allene and
574        propyne from room to high temperatures, J. Mol. Spectrosc., 305, 10-16, 2014.
575    Esler, M. B., Griffith, D. W. T., Wilson, S. R., and Steele, L. P.: Precision trace gas analysis by FT-IR
576        spectroscopy. 1. Simultaneous analysis of $CO_2$, $CH_4$, $N_2O$, and CO in air, Anal. Chem., 72, 206-215,
577        2000.
578    Fairburn, J. A., Behie, L. A., and Svrcek, W. Y.: Ultrapyrolysis of n-hexadecane in a novel micro-reactor,
579        Fuel, 69, 1537-1545, 1990.
580    Fang, M. X., Shen, D. K., Li, Y. X., Yu, C. J., Luo, Z. Y., and Cen, K. F.: Kinetic study on pyrolysis and
581        combustion of wood under different oxygen concentrations by using TG-FTIR analysis, J. Anal. Appl.
582        Pyrolysis, 77, 22-27, 2006.

Fernandes, P. M., and Botelho, H. S.: A review of prescribed burning effectiveness in fire hazard reduction, Int. J. Wildland Fire, 12, 117-128, 2003.

Finlayson-Pitts, B. J., Pitts Jr, J. N., and Lloyd, A. C.: Comment on" A study of the stability of methanol-fueled vehicle emissions in Tedlar bags", Environ. Sci. Technol., 26, 1668-1670, 1992.

Frenklach, M., Taki, S., Durgaprasad, M. B., and Matula, R. A.: Soot formation in shock-tube pyrolysis of acetylene, allene, and 1, 3-butadiene, Combust. Flame, 54, 81-101, 1983.

Frenklach, M., Yuan, T., and Ramachandra, M. K.: Soot formation in binary hydrocarbon mixtures, Energy Fuels, 2, 462-480, 1988.

Ghosh, P. N., and Günthard, H. H.: *Cis* and *trans* methyl nitrite: Gas phase ir spectra, band envelope analysis, hot band progressions and assignments, Spectrochim. Acta A Mol. Spectrosc., 37, 347-363, 1981.

Gilman, J. B., Lerner, B. M., Kuster, W. C., Goldan, P. D., Warneke, C., Veres, P. R., Roberts, J. M., de Gouw, J. A., Burling, I. R., and Yokelson, R. J.: Biomass burning emissions and potential air quality impacts of volatile organic compounds and other trace gases from fuels common in the US, Atmos. Chem. Phys., 15, 13915-13938, 2015.

Goode, J. G., Yokelson, R. J., Susott, R. A., and Ward, D. E.: Trace gas emissions from laboratory biomass fires measured by open-path Fourier transform infrared spectroscopy: Fires in grass and surface fuels, J. Geophys. Res. Atmos., 104, 21237-21245, 1999.

Goode, J. G., Yokelson, R. J., Ward, D. E., Susott, R. A., Babbitt, R. E., Davies, M. A., and Hao, W. M.: Measurements of excess $O_3$, $CO_2$, CO, $CH_4$, $C_2H_4$, $C_2H_2$, HCN, NO, $NH_3$, HCOOH, $CH_3COOH$, HCHO, and $CH_3OH$ in 1997 Alaskan biomass burning plumes by airborne Fourier transform infrared spectroscopy (AFTIR), J. Geophys. Res. Atmos., 105, 22147-22166, 2000.

Gordon, I. E., Rothman, L. S., Hill, C., Kochanov, R. V., Tan, Y., Bernath, P. F., Birk, M., Boudon, V., Campargue, A., Chance, K. V., Drouin, B. J., Flaud, J.-M., Gamache, R. R., Hodges, J. T., Jacquemart, D., Perevalov, V. I., Perrin, A., Shine, K. P., Smith , M.-A. H., Tennyson, J., Toon, G. C., Tran, H., Tyuterev, V. G., Barbe, A., Császár, A. G., Devi, V. M., Furtenbacher, T., Harrison, J. J., Hartmann, J.-M., Jolly, A., Johnson, T. J., Karman, T., Kleiner, I., Kyuberis, A. A., Loos, J., Lyulin, O. M., Massie, S. T., Mikhailenko, S. N., Moazzen-Ahmadi, N., Müller, H. S. P., Naumenko, O. V., Nikitin, A. V., Polyansky, O. L., Rey, M., Rotger, M., Sharpe, S. W., Sung, K., Starikova, D., S.A.Tashkun, S. A., VanderAuwera, J., Wagner, G., Wilzewski, J., Wcisło, P., Yu, S., and Zak, E. J.: The HITRAN2016 molecular spectroscopic database, J. Quant. Spectrosc. Radiat. Transfer, 203, 3-69, 2017.

Griffith, D. W. T.: Synthetic calibration and quantitative analysis of gas-phase FT-IR spectra, Appl. Spectrosc., 50, 59-70, 1996.

Griffith, D. W. T., Jones, N. B., McNamara, B., Walsh, C. P., Bell, W., and Bernardo, C.: Intercomparison of NDSC ground-based solar FTIR measurements of atmospheric gases at Lauder, New Zealand, J. Atmospheric Ocean. Technol., 20, 1138-1153, 2003.

Griffith, D. W. T., and Jamie, I. M.: Fourier Transform Infrared Spectrometry in Atmospheric and Trace Gas Analysis, Encyclopedia of Analytical Chemistry: Applications, Theory and Instrumentation, 2006.

Griffiths, J. F., Gilligan, M. F., and Gray, P.: Pyrolysis of isopropyl nitrate. I. Decomposition at low temperatures and pressures, Combust. Flame, 24, 11-19, 1975.

Hamada, Y., Nishimura, Y., and Tsuboi, M.: Infrared spectrum of *trans*-acrolein, Chem. Phys., 100, 365-375, 1985.

Hatch, L. E., Yokelson, R. J., Stockwell, C. E., Veres, P. R., Simpson, I. J., Blake, D. R., Orlando, J. J., and Barsanti, K. C.: Multi-instrument comparison and compilation of non-methane organic gas emissions from biomass burning and implications for smoke-derived secondary organic aerosol precursors, Atmos. Chem. Phys., 17, 1471-1489, 2017.

Herget, W. F., and Brasher, J. D.: Remote measurement of gaseous pollutant concentrations using a mobile Fourier transform interferometer system, Appl. Opt., 18, 3404-3420, 1979.

Hollenstein, H., and Günthard, H. H.: Solid state and gas infrared spectra and normal coordinate analysis of 5 isotopic species of acetaldehyde, Spectrochim. Acta A Mol. Spectrosc., 27, 2027-2060, 1971.

634 Hosseini, S., Shrivastava, M., Qi, L., Weise, D. R., Cocker, D. R., Miller, J. W., and Jung, H. S.: Effect of
635     low-density polyethylene on smoke emissions from burning of simulated debris piles, J. Air Waste
636     Manag. Assoc., 64, 690-703, 2014.
637 Jia, C., and Batterman, S.: A critical review of naphthalene sources and exposures relevant to indoor and
638     outdoor air, Int. J. Environ. Res. Public Health, 7, 2903-2939, 2010.
639 Johnson, T. J., Wienhold, F. G., Burrows, J. P., and Harris, G. W.: Frequency modulation spectroscopy at
640     1.3 μm using InGaAsP lasers: a prototype field instrument for atmospheric chemistry research, Appl.
641     Opt., 30, 407-413, 1991.
642 Johnson, T. J., Masiello, T., and Sharpe, S. W.: The quantitative infrared and NIR spectrum of $CH_2I_2$
643     vapor: vibrational assignments and potential for atmospheric monitoring, Atmos. Chem. Phys., 6,
644     2581-2591, 2006.
645 Johnson, T. J., Sams, R. L., Burton, S. D., and Blake, T. A.: Absolute integrated intensities of vapor-
646     phase hydrogen peroxide ($H_2O_2$) in the mid-infrared at atmospheric pressure, Anal. Bioanal. Chem.,
647     395, 377-386, 2009.
648 Johnson, T. J., Sams, R. L., Profeta, L. T., Akagi, S. K., Burling, I. R., Yokelson, R. J., and Williams, S.
649     D.: Quantitative IR spectrum and vibrational assignments for glycolaldehyde vapor: glycolaldehyde
650     measurements in biomass burning plumes, J. Phys. Chem. A, 117, 4096-4107, 2013.
651 Jonsson, A., and Bertilsson, B. M.: Formation of methyl nitrite in engines fueled with gasoline/methanol
652     and methanol/diesel, Environ. Sci. Technol., 16, 106-110, 1982.
653 Kabbadj, Y., Herman, M., Di Lonardo, G., Fusina, L., and Johns, J. W. C.: The bending energy levels of
654     $C_2H_2$, J. Mol. Spectrosc., 150, 535-565, 1991.
655 Karl, T. G., Christian, T. J., Yokelson, R. J., Artaxo, P., Hao, W. M., and Guenther, A.: The Tropical
656     Forest and Fire Emissions Experiment: method evaluation of volatile organic compound emissions
657     measured by PTR-MS, FTIR, and GC from tropical biomass burning, Atmos. Chem. Phys., 7, 5883-
658     5897, 2007.
659 Koss, A. R., Sekimoto, K., Gilman, J. B., Selimovic, V., Coggon, M. M., Zarzana, K. J., Yuan, B.,
660     Lerner, B. M., Brown, S. S., Jimenez, J. L., Krechmer, J., Roberts, J. M., Warneke, C., Yokelson, R. J.,
661     and de Gouw, J.: Non-methane organic gas emissions from biomass burning: identification,
662     quantification, and emission factors from PTR-ToF during the FIREX 2016 laboratory experiment,
663     Atmos. Chem. Phys., 18, 3299, 2018.
664 Lifshitz, A., Frenklach, M., and Burcat, A.: Structural isomerization $CH_2$=C=$CH_2$ ⇄ $CH_3$–C≡CH. Studies
665     with a single pulse shock tube, J. Phys. Chem., 79, 1148-1152, 1975.
666 Lifshitz, A., Frenklach, M., and Burcat, A.: Pyrolysis of allene and propyne behind reflected shocks, J.
667     Phys. Chem., 80, 2437-2443, 1976.
668 Lindenmaier, R., Williams, S. D., Sams, R. L., and Johnson, T. J.: Quantitative infrared absorption
669     spectra and vibrational assignments of crotonaldehyde and methyl vinyl ketone using gas-phase mid-
670     infrared, far-infrared, and liquid raman spectra: *s-cis* vs *s-trans* composition confirmed via temperature
671     studies and *ab initio* methods, J. Phys. Chem. A, 121, 1195-1212, 2017.
672 Liu, W.-J., Li, W.-W., Jiang, H., and Yu, H.-Q.: Fates of chemical elements in biomass during its
673     pyrolysis, Chem. Rev., 117, 6367-6398, 2017.
674 Lobert, J. M., Scharffe, D. H., Weimin, H., Kuhlbusch, T. A., Seuwen, R., Warneck, P., and Crutzen, P.
675     J.: Experimental evaluation of biomass burning emissions: Nitrogen and carbon containing
676     compounds, in: Global Biomass Burning: Atmospheric, Climatic, and Biospheric Implications, 1991.
677 Lord, R. C., and Venkateswarlu, P.: The Rotation-Vibration Spectra of Allene and Allene-d4, J. Chem.
678     Phys., 20, 1237-1247, 1952.
679 Lu, M., and Mulholland, J. A.: PAH growth from the pyrolysis of CPD, indene and naphthalene mixture,
680     Chemosphere, 55, 605-610, 2004.
681 Mertz, L.: Auxiliary computation for Fourier spectrometry, Infrared Phys., 7, 17-23, 1967.
682 Miller, J. D., Safford, H. D., Crimmins, M., and Thode, A. E.: Quantitative evidence for increasing forest
683     fire severity in the Sierra Nevada and southern Cascade Mountains, California and Nevada, USA,
684     Ecosystems, 12, 16-32, 2009.

685 Phillips, M. C., Taubman, M. S., Bernacki, B. E., Cannon, B. D., Stahl, R. D., Schiffern, J. T., and Myers,
686     T. L.: Real-time trace gas sensing of fluorocarbons using a swept-wavelength external cavity quantum
687     cascade laser, Analyst, 139, 2047-2056, 2014.
688 Profeta, L. T. M., Sams, R. L., Johnson, T. J., and Williams, S. D.: Quantitative infrared intensity studies
689     of vapor-phase glyoxal, methylglyoxal, and 2, 3-butanedione (diacetyl) with vibrational assignments,
690     J. Phys. Chem. A, 115, 9886-9900, 2011.
691 Richter, H., and Howard, J. B.: Formation of polycyclic aromatic hydrocarbons and their growth to
692     soot—a review of chemical reaction pathways, Prog. Energy Combust. Sci., 26, 565-608, 2000.
693 Safdari, M.-S., Rahmati, M., Amini, E., Howarth, J. E., Berryhill, J. P., Dietenberger, M., Weise, D. R.,
694     and Fletcher, T. H.: Characterization of pyrolysis products from fast pyrolysis of live and dead
695     vegetation native to the Southern United States, Fuel, 229, 151-166, 2018.
696 Schmeltz, I., and Hoffmann, D.: Nitrogen-containing compounds in tobacco and tobacco smoke, Chem.
697     Rev., 77, 295-311, 1977.
698 Selimovic, V., Yokelson, R. J., Warneke, C., Roberts, J. M., Gouw, J. d., Reardon, J., and Griffith, D. W.
699     T.: Aerosol optical properties and trace gas emissions by PAX and OP-FTIR for laboratory-simulated
700     western US wildfires during FIREX, Atmos. Chem. Phys., 18, 2929-2948, 2018.
701 Sharpe, S. W., Johnson, T. J., Sams, R. L., Chu, P. M., Rhoderick, G. C., and Johnson, P. A.: Gas-phase
702     databases for quantitative infrared spectroscopy, Appl. Spectrosc., 58, 1452-1461, 2004.
703 Smith, T. E. L., Wooster, M. J., Tattaris, M., and Griffith, D. W. T.: Absolute accuracy and sensitivity
704     analysis of OP-FTIR retrievals of $CO_2$, $CH_4$ and CO over concentrations representative of "clean air"
705     and "polluted plumes", Atmos. Meas. Tech., 4, 97-116, 2011.
706 Stein, Y. S., Antal Jr, M. J., and Jones jr, M.: A study of the gas-phase pyrolysis of glycerol, J. Anal.
707     Appl. Pyrolysis, 4, 283-296, 1983.
708 Stockwell, C. E., Yokelson, R., Kreidenweis, S. M., Robinson, A. L., DeMott, P. J., Sullivan, R. C.,
709     Reardon, J., Ryan, K. C., Griffith, D. W. T., and Stevens, L.: Trace gas emissions from combustion of
710     peat, crop residue, domestic biofuels, grasses, and other fuels: configuration and Fourier transform
711     infrared (FTIR) component of the fourth Fire Lab at Missoula Experiment (FLAME-4), Atmos. Chem.
712     Phys., 14, 9727-9754, 2014.
713 Taghizadeh, M. T., Yeganeh, N., and Rezaei, M.: The investigation of thermal decomposition pathway
714     and products of poly (vinyl alcohol) by TG-FTIR, J. Appl. Polym. Sci., 132, 2015.
715 Talbot, R. W., Beecher, K. M., Harriss, R. C., and Cofer, W. R.: Atmospheric geochemistry of formic and
716     acetic acids at a mid-latitude temperate site, J. Geophys. Res. Atmos., 93, 1638-1652, 1988.
717 Taubman, M. S., Myers, T. L., Cannon, B. D., and Williams, R. M.: Stabilization, injection and control of
718     quantum cascade lasers, and their application to chemical sensing in the infrared, Spectrochim. Acta A
719     Mol. Biomol. Spectrosc., 60, 3457-3468, 2004.
720 Turetsky, M. R., Kane, E. S., Harden, J. W., Ottmar, R. D., Manies, K. L., Hoy, E., and Kasischke, E. S.:
721     Recent acceleration of biomass burning and carbon losses in Alaskan forests and peatlands, Nat.
722     Geosci., 4, 27, 2011.
723 Urbanski, S. P., Hao, W. M., and Baker, S.: Chemical composition of wildland fire emissions,
724     Developments in Environmental Science, 8, 79-107, 2008.
725 Wagner, N. L., Dubé, W. P., Washenfelder, R. A., Young, C. J., Pollack, I. B., Ryerson, T. B., and
726     Brown, S. S.: Diode laser-based cavity ring-down instrument for $NO_3$, $N_2O_5$, NO, $NO_2$ and $O_3$ from
727     aircraft, Atmos. Meas. Tech., 4, 1227-1240, 2011.
728 Wagner, R., Fine, J., Simmons, J. W., and Goldstein, J. H.: Microwave Spectrum, Structure, and Dipole
729     Moment of *s-trans* Acrolein, J. Chem. Phys., 26, 634-637, 1957.
730 Ward, D. E., and Hardy, C. C.: Smoke emissions from wildland fires, Environ. Int., 17, 117-134, 1991.
731 Weise, D. R., Johnson, T. J., and Reardon, J.: Particulate and trace gas emissions from prescribed burns in
732     southeastern US fuel types: Summary of a 5-year project, Fire Saf. J., 74, 71-81, 2015.
733 White, J. U.: Long optical paths of large aperture, JOSA, 32, 285-288, 1942.
734 Williams, P. T., and Williams, E. A.: Fluidised bed pyrolysis of low density polyethylene to produce
735     petrochemical feedstock, J. Anal. Appl. Pyrolysis, 51, 107-126, 1999.

736 Yokelson, R. J., Griffith, D. W. T., and Ward, D. E.: Open-path Fourier transform infrared studies of
737     large-scale laboratory biomass fires, J. Geophys. Res. Atmos., 101, 21067-21080, 1996.
738 Yokelson, R. J., Susott, R., Ward, D. E., Reardon, J., and Griffith, D. W. T.: Emissions from smoldering
739     combustion of biomass measured by open-path Fourier transform infrared spectroscopy, J. Geophys.
740     Res. Atmos., 102, 18865-18877, 1997.
741 Yokelson, R. J., Crounse, J. D., DeCarlo, P. F., Karl, T., Urbanski, S. P., Atlas, E., Campos, T.,
742     Shinozuka, Y., Kasputin, V., Clarke, A. D., Weinheimer, A., Knapp, D. J., Montzka, D. D., Holloway,
743     J., Weibring, P., Flocke, F., Zheng, W., Toohey, D., Wennberg, P. O., Wiedinmyer, C., Mauldin, L.,
744     Fried, A., Richter, D., Walega, J., Jimenez, J. L., Adachi, K., Buseck, P. R., Hall, S. R., and Shetter,
745     R.: Emissions from biomass burning in the Yucatan, Atmos. Chem. Phys., 9, 5785, 2009.
746 Yokelson, R. J., Burling, I. R., Gilman, J. B., Warneke, C., Stockwell, C. E., Gouw, J. d., Akagi, S. K.,
747     Urbanski, S. P., Veres, P., Roberts, J. M., Kuster, W. C., Reardon, J., Griffith, D. W. T., Johnson, T. J.,
748     Hosseini, S., Miller, J. W., Cocker III, D. R., Jung, H., and Weise, D. R.: Coupling field and laboratory
749     measurements to estimate the emission factors of identified and unidentified trace gases for prescribed
750     fires, Atmos. Chem. Phys., 13, 89-116, 2013.

751
752

753

754

755

756

757

758